Rheology of dense granular flows for elongated particles

Dániel B. Nagy,[1] Philippe Claudin,[2] Tamás Börzsönyi,[1] and Ellák Somfai[1,*]

[1]*Institute for Solid State Physics and Optics, Wigner Research Center for Physics, Hungarian Academy of Sciences, P.O. Box 49, H-1525 Budapest, Hungary*

[2]*Physique et Mécanique des Milieux Hétérogènes, PMMH UMR 7636, ESPCI–CNRS–Université Paris-Diderot–Université Pierre-et-Marie-Curie, 10 rue Vauquelin, 75005 Paris, France*

(Received 16 June 2017; published 4 December 2017)

We study the rheology of dense granular flows for frictionless spherocylinders by means of 3D numerical simulations. As in the case of spherical particles, the effective friction μ is an increasing function of the inertial number I, and we systematically investigate the dependence of μ on the particle aspect ratio Q, as well as that of the normal stress differences, the volume fraction, and the coordination number. We show in particular that the quasistatic friction coefficient is nonmonotonic with Q: from the spherical case $Q = 1$, it first sharply increases, reaches a maximum around $Q \simeq 1.05$, and then gently decreases until $Q = 3$, passing its initial value at $Q \simeq 2$. We provide a microscopic interpretation for this unexpected behavior through the analysis of the distribution of dissipative contacts around the particles: as compared to spheres, slightly elongated grains enhance contacts in their central cylindrical band, whereas at larger aspect ratios particles tend to align and dissipate by preferential contacts at their hemispherical caps.

DOI: 10.1103/PhysRevE.96.062903

I. INTRODUCTION

Rheology of dense granular flows is an active domain of research, motivated by fundamental questions on this "complex fluid" as well as by practical needs in soil mechanics and geotechnical engineering. Since the 1950s a number of models have been suggested, including Bagnold's scaling [1,2], the theory of the rapid flow regime [3], and other regimes [4]. A major step in the description of the dense regime was achieved 10–15 years ago with the development of the framework of the now so-called $\mu(I)$ rheology [5,6], which successfully describes these flows in the absence of strong spatial gradients or temporal changes. This approach has shown that the constitutive equations, which augment the conservation laws for a complete rheological description of these flows, can be formalized in terms of the "inertial number" $I = \dot{\gamma} d/\sqrt{p/\rho}$, where $\dot{\gamma}$ is the shear rate, p is the pressure, d is the average grain diameter, and ρ is the density of the particles' material. This dimensionless number can be interpreted as the ratio of the characteristic time scale $d/\sqrt{p/\rho}$ of microscopic rearrangements and the macroscopic time scale $1/\dot{\gamma}$ of the deformation. In the case of rigid grains, for which the pressure is the only stress scale, the dimensional analysis tells us that the effective friction μ of the flow, defined by the ratio of the shear stress to the pressure, and the volume fraction ϕ of the granular packing are functions of I. The shape of these functions has been determined both by simulations [7–9] and experiments [10,11].

The $\mu(I)$ formalism has been successfully applied in a number of flow geometries [5], recovering the Bagnold scaling in flows down an inclined plane [2] and describing chute flow [12–15], silo discharge [16], granular column collapse [17,18], and dynamic compressibility effects in spontaneous oscillatory motion [19,20]. This rheology has been extended in a number of ways, taking into account various effects like cohesion [21], finite pressure or soft particles [22], and self-propelling particles [23]. Another example for extension is the description of granular suspensions [24–26]. In this case, a new time scale, that of the viscous dissipation, is introduced, which is captured by a new dimensionless group, the "viscous number" J. This formalism describes Brownian suspensions as well [27] and has been incorporated to diphasic models for sediment transport [28–30].

Another trend in granular physics is considering shape anisotropy for the particles; see the recent review [31] and references therein. One of the fundamental results is the observation that elongated particles get oriented in shear flow [32–35]. The average orientation angle θ_{av}, which is the angle between the average orientation of the particles and the streamlines, is nonzero; it decreases with the length-to-width aspect ratio Q of the particles, but only weakly depends on the shear rate [36]. There is an interplay between this orientational ordering and the packing fraction or the contact force network [37–39]. The quasistatic behavior of two-dimensional (2D) systems has been investigated with rounded-cap rectangular particles in a biaxial setup [37]. The fast regime (typically $I > 0.1$) has been explored in various 2D configurations, including a volume-fraction-controlled shear cell, with dumbbells [40,41]. In this paper, we study the rheological properties of assemblies of 3D frictionless spherocylinders in a pressure-controlled shear cell. We explore the range of shear rate for which the $\mu(I)$ formalism is expected to apply, i.e., from the quasistatic limit ($I \to 0$) to the beginning of the kinetic regime $I \simeq 0.1$. We unexpectedly find a nonmonotonic behavior of the quasistatic friction coefficient with the particle aspect ratio, a key result missed by previous studies [37,41]. We also report the emergence of normal stress differences, whose marginal presence was already noticed for 3D flows of spheres [42], but which clearly develop for elongated particles in a way qualitatively similar to those in suspensions of fibers [43,44]. A very recent experimental study of the rheology of noncolloidal suspensions of rigid fibers has investigated the effect of the particle aspect ratio in the

*somfai.ellak@wigner.mta.hu

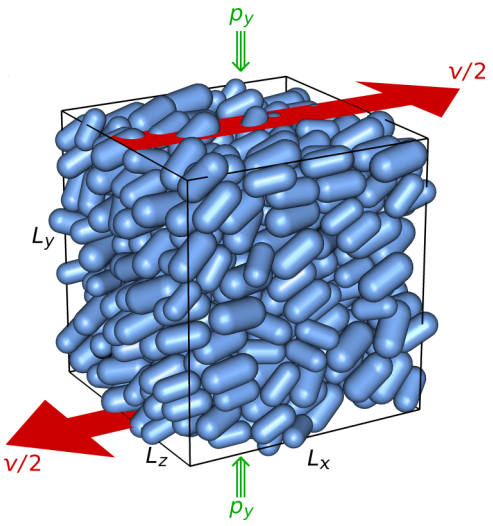

FIG. 1. The simulation box, here containing 500 spherocylindrical particles of aspect ratio $Q = 2$ in the stationary state, is sheared in the x direction. A feedback loop adjusts L_y to ensure a controlled applied stress $-p_y$ in the y direction. The shear rate is $\dot{\gamma} = v/L_y$.

range 3–15, indicating an aspect ratio independent friction coefficient, but a decreasing jamming packing fraction with increasing Q [45]. A nonmonotonic dependence of the packing fraction on Q has been observed previously also in nonsheared systems [46–48].

II. NUMERICAL SETUP

To model homogenous shear flow, we used a 3D plane-Couette geometry, with periodic boundary conditions in the x (flow) and z (neutral) directions and Lees-Edwards boundary conditions in the y (velocity gradient) direction (Fig. 1); this way undesirable effects of walls could be eliminated [49]. Instead of cylinders [50] we chose the spherocylindical shape, because of the availability of efficient numerical algorithms [51] and continuous transition to the reference spherical shape. The spherocylinders were parametrized by their length-to-diameter aspect ratio $Q = \ell/2R$. The repulsive force $\mathbf{F}_{ij}$ between particles i and j was proportional to their normal overlap, and we employed a viscous velocity-difference-based term for dissipation: $\mathbf{F}_{ij} = (-k\,\delta_{ij} + b\,\mathbf{v}_{c,ij}\cdot\hat{c}_{ij})\,\hat{c}_{ij}$, where δ_{ij} and $\hat{c}_{ij}$ are the magnitude and unit direction vector of the normal overlap between the particles, and for the velocity difference $\mathbf{v}_{c,ij}$ at contact the rotation of the particles was taken into account as well. There is no tangential component of the force that would result from a Coulombic contact friction. The stiffness k of the contacts, the particle diameter $2R$, and the density ρ were set to unity, implicitly defining the length, time, and mass units of the simulation. Importantly, some polydispersity is introduced to reduce the effects of crystallization at large Q, and while we kept the aspect ratio constant, we have drawn the radii of the particles from a uniform distribution with a ratio of standard deviation to mean of 10%. The prefactor b in the dissipative term was set by specifying a given restitution coefficient for binary collision. The equations of motion were integrated by the velocity-Verlet scheme, representing particle rotations by quaternions [52].

We created the initial conditions of random particle orientation with overdamped dynamics and afterwards sheared the system at constant shear rate $\dot{\gamma}$. During shear we employed stress control, where one side of the box, L_y, was adjusted by a feedback loop such that the corresponding normal stress σ_{yy} fluctuated around a specified value $-p_y$. We have used $p_y = 10^{-3}$ in these units, corresponding to the rigid limit where rescaled results become independent of p_y. We kept L_x and L_z fixed in order to avoid the development of a singular box shape due to normal stress differences. All measurements were taken in the stationary state, reached after a deformation of $\gamma = 25$ when starting from the initial conditions or of $\gamma = 10$ from the stationary state of a different shear rate. All quantities of interest were time-averaged at least over an additional deformation of $\gamma = 5$. In the steady state, the packing fraction as well as all stress components σ_{ij} were homogenous, and the velocity profile was linear (no shear banding). Finally, we checked that our results were independent of the integration time step, set to $1/100$ of the duration of a binary collision, and qualitatively insensitive to the value of the restitution coefficient in the range 0.3–0.7, and here set to 0.5.

III. RESULTS

We measured the inertial number dependence of different quantities. In Fig. 2(a) we show the effective friction $\mu = \sigma_{xy}/p_y$ vs I for spherocylinders of a few selected aspect ratios and for spheres for reference. (Note that in the definition of I we used the value p_y, controlling the stress, instead of the pressure p.) Similarly to Ref. [26], we fitted the empirical form

$$\mu(I) \approx \mu_c + \mu_1 I^{\alpha}\,, \tag{1}$$

allowing us to extrapolate to the quasistatic friction μ_c in the $I \to 0$ limit. Best fitting is of course obtained when all three parameters are adjusted, but we then fixed the exponent to its average, $\alpha = 0.4$, yielding less noisy data with a two-parameter fit (μ_c and μ_1). This value of α is in agreement with that deduced from 3D simulations of frictionless hard spheres [53] and similar to the exponent 0.5 observed for frictionless circles [54]. Figure 2(d) displays the aspect ratio dependence of μ_c, showing a surprising nonmonotonic function: it rises steeply for aspect ratios slightly larger than one and takes the highest value around $Q = 1.05$, followed by a slow decrease—we give a microscopic interpretation of this behavior later. Similarly, we show the normalized first and second normal stress differences $N_1/p_y = (\sigma_{xx} - \sigma_{yy})/p_y$ and $N_2/p_y = (\sigma_{yy} - \sigma_{zz})/p_y$ in Figs. 2(b) and 2(c). Their quasistatic values, extrapolated with a fit like Eq. (1) (also with fixed $\alpha = 0.4$), are shown in Figs. 2(e) and 2(f). As expected, the quasistatic first normal stress difference vanishes for spheres and increases close to linearly for aspect ratios of $Q \lessapprox 2.5$. The second normal stress difference is negative, although 2–3 times smaller in amplitude than N_1 (even for spheres $N_{2c}/p_y \simeq 1\%$), and has a very strong aspect ratio dependence for nearly spherical particles.

In complement to the stress behaviors, we show the volume fraction in Fig. 3(a). As for spheres, ϕ decreases with I as larger shear rates generate a more dilute system. Also, consistently with what has been observed for spherocylinders [46] and ellipsoids [47] in nonsheared systems, the volume fraction of

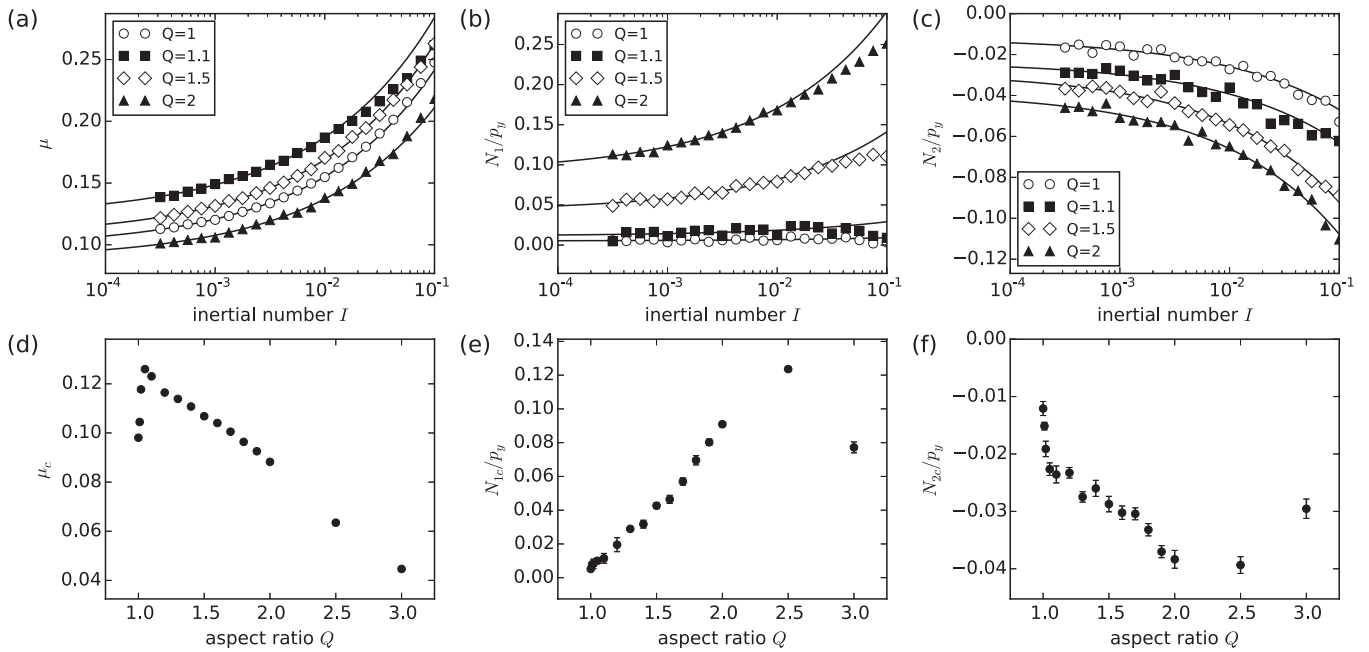

FIG. 2. Top row: (a) effective friction and (b) first and (c) second normal stress differences, as functions of I. The normal stress differences are normalized by the absolute value of the imposed stress, p_y. The solid curves are fits of Eq. (1) with $\alpha = 0.4$ in the range $10^{-3.5} \leqslant I \leqslant 10^{-2}$. Bottom row: Aspect ratio dependence of the quasistatic ($I \to 0$) values of the same quantities: (d) effective friction and (e) first and (f) second normal stress differences. The first few points correspond to $Q = 1$, 1.01, 1.02, 1.05, and 1.1.

elongated particles first quickly increases with Q, followed by a slow decrease—the behavior beyond $Q \gtrapprox 2.5$ is discussed later. Finally, we computed the coordination number Z. A static packing of frictionless hard spheres takes the isostatic value 6. Once the particles become elongated, due to the two extra rotation degrees of freedom per particle, this value jumps to 10. In Fig. 3(b) we plot the measured values. For spheres, Z_c is slightly larger than 6 due to the finite pressure, or equivalently the softness of the particles. For increasing aspect ratio, Z_c increases initially sharply but continuously, reaching a flat maximum around $Q \approx 1.8$. The inset shows the inertial number dependence, demonstrating an expected decrease of contacts for more violent flows.

Next we look at the orientational order induced by the shear deformation. Figure 4 shows, for a few selected aspect ratios, the distribution of the angle θ between the streamlines (x axis) and the projection of the particle axis onto the x-y shear plane. For more elongated particles the distribution is narrower and its mode and mean are closer to zero. The average angle $\theta_{\rm av}$ is slightly off the mode due to asymmetry of the distribution. The aspect ratio dependence of $\theta_{\rm av}$ and the nematic order parameter S, which is defined as the largest eigenvalue of the order tensor, are shown in the inset: increasing Q results in increasing S and reducing $\theta_{\rm av}$, in almost linear fashions. Note that even the smallest aspect ratio considered, $Q = 1.01$, has a small but finite nematic order, with $\theta_{\rm av} \simeq 45^\circ$.

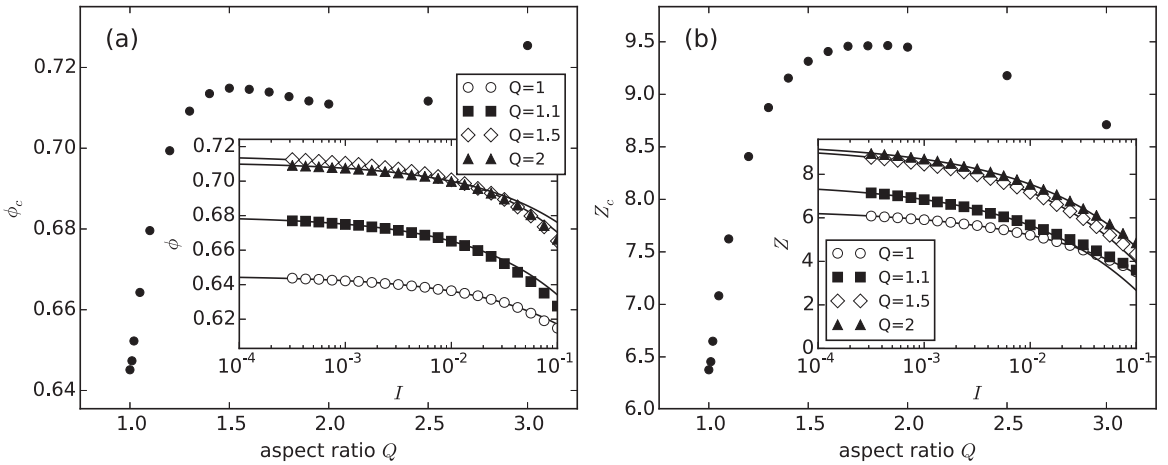

FIG. 3. The aspect ratio dependence of the quasistatic values of (a) the volume fraction and (b) the coordination number. Insets: I dependencies for a few Q values. Solid lines: Fits of Eq. (1), with respective fixed exponents 0.4 and 0.5.

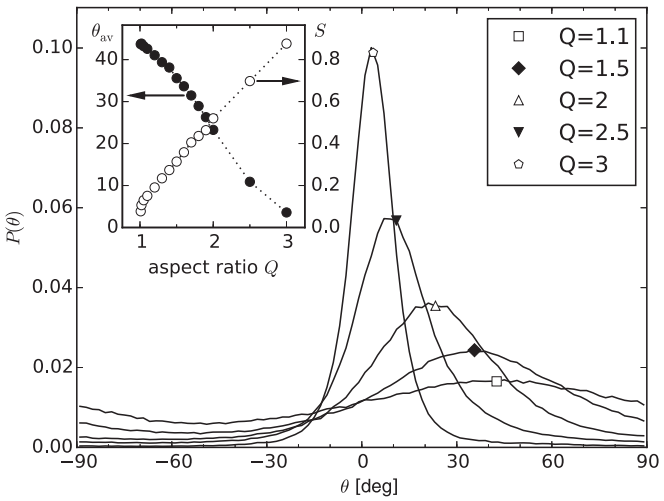

FIG. 4. Orientation distributions for five different aspect ratios (see legend). The symbols locate the average orientation θ_{av}. Inset: Average orientation θ_{av} (black bullets, left axis) and nematic order parameter S (white circles, right axis) as functions of Q. These data are for $I = 3.16 \times 10^{-4}$.

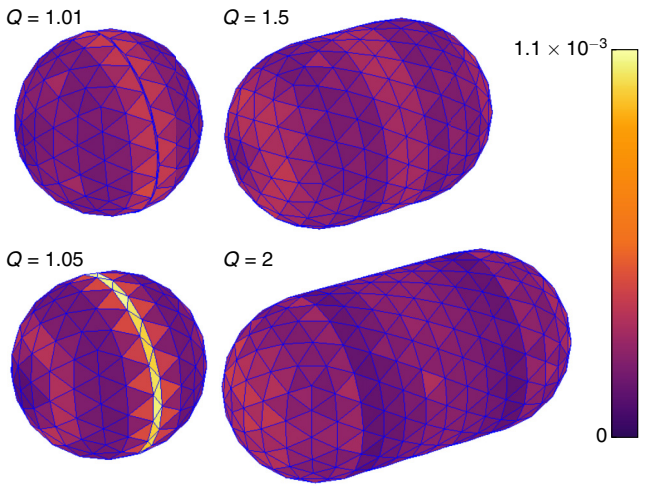

FIG. 5. Average dissipative power per unit area visualized on a discrete mesh for four aspect ratios (see legends and color code). Dissipation at each contact is accumulated in triangular bins, such that the axes of the differently oriented particles are turned into a canonical orientation, in which the mesh is defined. These data are for $I = 3.16 \times 10^{-4}$.

Finally we determined which region of the particles' surface is most responsible for dissipation (Fig. 5). The highest dissipation density was observed in the cylindrical band of the $Q = 1.05$ spherocylinder. More spherical particles showed a more homogenous distribution, but the slight enhancement of the dissipation near the cylindrical band is visible even for $Q = 1.01$. For more elongated particles, the dissipation becomes dominated at the hemispherical caps.

IV. DISCUSSION AND PERSPECTIVES

The framework of the $\mu(I)$ rheology can be extended to elongated particles. The aspect ratio dependence of the rheological quantities display two remarkable features: (i) the dissipation, quantified by μ_c, is maximal around $Q = 1.05$, and (ii) the normal stress differences, the volume fraction as well as the coordination number, behave nonmonotonically for $Q \gtrapprox 2.5$.

Issue (i) is closely related to the highest observed density of dissipation in the cylindrical band of the $Q = 1.05$ particles. We suspect that this effect is particularly strong for spherocylindrical particles, where the surface is not analytic (one of the curvatures is not continuous). An analysis similar to what is shown in Fig. 5 revealed that not only the dissipation density but also the contact density is increased in that region: a larger than expected number of particle pairs locked in a configuration where the contact is carried by the cylindrical region for at least one of the particles. We explain issue (ii) by the high nematic and partial spatial order observed for sufficiently elongated frictionless spherocylinders. While the introduction of polydispersity destroyed the crystalline order perpendicular to the streamlines, we still observe short-range chains of particles which follow each other on a streamline. This can also explain why the tips of the particles become the dominant location for dissipation for the more elongated particles.

The robustness of these results should be assessed by complementary simulations, e.g., in 2D, with other shapes like ellipses, possibly including frictional contacts, as well as by experiments [45,55]. A better understanding of the large Q behavior probably requires the use of larger systems, and here our data for $Q = 3$ may be affected by a too small size. This issue motivates further studies towards the flow of fibers and entangled materials [48], whose rich mechanics suggest interesting rheological properties.

ACKNOWLEDGMENTS

We thank A. Favier de Coulomb, D. Kálmán, B. Andreotti, E. Clément, O. Pouliquen, A. Lindner, B. Szabó, and M. Trulsson for useful discussions. This work was supported by the Hungarian National Research, Development and Innovation Office (NKFIH), under Grant No. OTKA K 116036, and the Hungarian-French bilateral TéT/Balaton exchange programme. We acknowledge computational resources provided by NIIF in Hungary at Debrecen.

[1] R. A. Bagnold, Proc. R. Soc. London, Ser. A **225**, 49 (1954).
[2] L. E. Silbert, D. Ertas, G. S. Grest, T. C. Halsey, D. Levine, and S. J. Plimpton, Phys. Rev. E **64**, 051302 (2001).
[3] J. T. Jenkins and S. B. Savage, J. Fluid Mech. **130**, 187 (1983).
[4] C. S. Campbell, J. Fluid Mech. **465**, 261 (2002).
[5] GDR MiDi, Eur. Phys. J. E **14**, 341 (2004).
[6] Y. Forterre and O. Pouliquen, Annu. Rev. Fluid Mech. **40**, 1 (2008).

[7] F. da Cruz, S. Emam, M. Prochnow, J.-N. Roux, and F. Chevoir, Phys. Rev. E **72**, 021309 (2005).
[8] P. Jop, Y. Forterre, and O. Pouliquen, Nature (London) **441**, 727 (2006).
[9] T. Hatano, Phys. Rev. E **75**, 060301 (2007).
[10] P. Jop, Y. Forterre, and O. Pouliquen, J. Fluid Mech. **541**, 167 (2005).
[11] A. Fall, G. Ovarlez, D. Hautemayou, C. Meziere, J.-N. Roux, and F. Chevoir, J. Rheol. **59**, 1065 (2015).
[12] J. M. N. T. Gray and A. N. Edwards, J. Fluid Mech. **755**, 503 (2014).
[13] T. Barker, D. G. Schaeffer, P. Bohorquez, and J. M. N. T. Gray, J. Fluid Mech. **779**, 794 (2015).
[14] J. L. Baker, T. Barker, and J. M. N. T. Gray, J. Fluid Mech. **787**, 367 (2016).
[15] T. Börzsönyi, R. E. Ecke, and J. N. McElwaine, Phys. Rev. Lett. **103**, 178302 (2009).
[16] L. Staron, P.-Y. Lagree, and S. Popinet, Eur. Phys. J. E **37**, 5 (2014).
[17] P.-Y. Lagree, L. Staron, and S. Popinet, J. Fluid Mech. **686**, 378 (2011).
[18] L. R. Ionescu, A. Mangeney, F. Bouchut, and O. Roche, J. Non-Newtonian Fluid Mech. **219**, 1 (2015).
[19] L. Staron, Phys. Rev. E **86**, 041307 (2012).
[20] M. Trulsson, M. Bouzid, P. Claudin, and B. Andreotti, Europhys. Lett. **103**, 38002 (2013).
[21] P. G. Rognon, J. N. Roux, D. Wolf, M. Naaim, and F. Chevoir, Europhys. Lett. **74**, 644 (2006).
[22] A. Favier de Coulomb, M. Bouzid, P. Claudin, E. Clément, and B. Andreotti, Phys. Rev. Fluids **2**, 102301 (2017).
[23] A. Peshkov, P. Claudin, E. Clement, and B. Andreotti, Europhys. Lett. **116**, 14001 (2016).
[24] F. Boyer, E. Guazzelli, and O. Pouliquen, Phys. Rev. Lett. **107**, 188301 (2011).
[25] M. Trulsson, B. Andreotti, and P. Claudin, Phys. Rev. Lett. **109**, 118305 (2012).
[26] E. DeGiuli, G. Düring, E. Lerner, and M. Wyart, Phys. Rev. E **91**, 062206 (2015).
[27] M. Trulsson, M. Bouzid, J. Kurchan, E. Clement, P. Claudin, and B. Andreotti, Europhys. Lett. **111**, 18001 (2015).
[28] M. Ouriemi, P. Aussillous, and E. Guazzelli, J. Fluid Mech. **636**, 295 (2009).
[29] P. Aussillous, J. Chauchat, M. Pailha, M. Medale, and E. Guazzelli, J. Fluid Mech. **736**, 594 (2013).
[30] F. Chiodi, P. Claudin, and B. Andreotti, J. Fluid Mech. **755**, 561 (2014).
[31] T. Börzsönyi and R. Stannarius, Soft Matter **9**, 7401 (2013).
[32] K. A. Reddy, V. Kumaran, and J. Talbot, Phys. Rev. E **80**, 031304 (2009).
[33] C. S. Campbell, Phys. Fluids **23**, 013306 (2011).
[34] T. Börzsönyi, B. Szabó, G. Törös, S. Wegner, J. Török, E. Somfai, T. Bien, and R. Stannarius, Phys. Rev. Lett. **108**, 228302 (2012).
[35] M. Boton, E. Azema, N. Estrada, F. Radjai, and A. Lizcano, Phys. Rev. E **87**, 032206 (2013).
[36] T. Börzsönyi, B. Szabó, S. Wegner, K. Harth, J. Török, E. Somfai, T. Bien, and R. Stannarius, Phys. Rev. E **86**, 051304 (2012).
[37] E. Azema and F. Radjai, Phys. Rev. E **81**, 051304 (2010).
[38] E. Azema and F. Radjai, Phys. Rev. E **85**, 031303 (2012).
[39] S. Wegner, R. Stannarius, A. Boese, G. Rose, B. Szabó, E. Somfai, and T. Börzsönyi, Soft Matter **10**, 5157 (2014).
[40] K. A. Reddy, J. Talbot, and V. Kumaran, J. Fluid Mech. **660**, 475 (2010).
[41] S. Mandal and D. V. Khakhar, Phys. Fluids **28**, 103301 (2016).
[42] M. Depken, J. B. Lechman, M. V. Hecke, W. V. Saarloos, and G. S. Grest, Europhys. Lett. **78**, 58001 (2007).
[43] B. Snook, L. M. Davidson, J. E. Butler, O. Pouliquen, and E. Guazzelli, J. Fluid Mech. **758**, 486 (2014).
[44] S. Bounoua, P. Kuzhir, and E. Lemaire, J. Rheol. **60**, 661 (2016).
[45] F. Tapia, S. Shaikh, J. E. Butler, O. Pouliquen, and E. Guazzelli, J. Fluid Mech. **827**, R5 (2017).
[46] S. R. Williams and A. P. Philipse, Phys. Rev. E **67**, 051301 (2003).
[47] A. Donev, I. Cisse, D. Sachs, E. Variano, F. H. Stillinger, R. Connelly, S. Torquato, and P. M. Chaikin, Science **303**, 990 (2004).
[48] D. Rodney, M. Fivel, and R. Dendievel, Phys. Rev. Lett. **95**, 108004 (2005).
[49] R. Artoni and P. Richard, Phys. Rev. Lett. **115**, 158001 (2015).
[50] Y. Guo, C. Wassgren, W. Ketterhagen, B. Hancock, B. James, and J. Curtis, J. Fluid Mech. **713**, 1 (2012).
[51] C. Vega and S. Lago, Comput. Chem. **18**, 55 (1994).
[52] I. P. Omelyan, Comput. Phys. **12**, 97 (1998).
[53] P.-E. Peyneau and J.-N. Roux, Phys. Rev. E **78**, 011307 (2008).
[54] M. Bouzid, M. Trulsson, P. Claudin, E. Clement, and B. Andreotti, Phys. Rev. Lett. **111**, 238301 (2013).
[55] M. Trulsson (unpublished).